ELSEVIER

Polymer 40 (1999) 2805–2812

polymer

Melting and crystallization of poly(ethylene-*co*-octene) measured by modulated d.s.c. and temperature-resolved X-ray diffraction

R. Androsch[1]

Martin-Luther-University Halle-Wittenberg, Institute of Materials Technology, Geusaer Str., 06217 Merseburg, Germany

Received 11 March 1998; revised 28 May 1998; accepted 10 June 1998

Abstract

The melting and crystallization behaviour of metallocene-catalysed commercial poly(ethylene-*co*-octene) was investigated by conventional and temperature-modulated differential scanning calorimetry (d.s.c. and TMd.s.c.) and by temperature-resolved wide angle X-ray scattering. The thermal behaviour of the copolymer is characterized by a very broad melting and crystallization range. Both the melting and the crystallization are complex transitions of at least two processes with different kinetics. On decreasing the temperature, crystallization starts with the formation of a separate crystalline phase and continues gradually with development of an amorphous–crystalline mesophase until the glass transition is reached. In TMd.s.c., the formation of the crystalline phase is seen as an irreversible, non-reversing process, whereas the glass transition gives a reversing heat flow signal. Similarly, on heating, the melting process is initiated after traversing the glass transition as a largely reversing process, followed by melting of the crystalline phase with non-reversing character in a narrower temperature range.

Keywords: Poly(ethylene-*co*-octene); Melting and crystallization; Glass transition

1. Introduction

In 1993 the DOW Chemical Company commercialized a new class of linear low density polyethylene (PE) under the trade name Engage. This copolymer of ethylene and octene is synthesized using new, homogeneous, single-site catalysts resulting in a uniform length of the branches, a very random distribution of the comonomer along the backbone, a unique distribution of the comonomer in different chains and a very narrow molecular weight distribution. The distribution of the comonomer along the backbone, the length of the branches and the comonomer concentration are important parameters of the chain configuration and are determining the crystallization behaviour, including the ultimate crystallinity of the polymer and, therefore, the macroscopic properties [1–3].

Due to the availability of PE copolymers with this well-defined chain architecture, investigations were performed to correlate the chain configuration (characteristics of branching) with the supermolecular structure (type, amount and quality of the crystalline as well as amorphous phases) and the macroscopic properties. The chain configuration is directly correlated to the density, which can be used to classify the copolymers: a density higher than 0.93 g cm^{-3} (0 mol% comonomer content) is correlated to PE with a typically lamellar and spherulitic superstructure. Samples with a density between 0.93 and 0.91 g cm^{-3} (approximately up to 3 mol% comonomer) show a finer lamellar and spherulitic morphology. In the density range between 0.91 and 0.89 g cm^{-3} (approximately up to 8 mol% comonomer) the material contains a mixture of lamellar and bundle-like crystals. Finally, a density lower than 0.89 g cm^{-3} is related exclusively to fringed-micellar structures [4]. Taking into account the density 0.852 g cm^{-3} of completely amorphous PE, the crystallinity can reach values of nearly zero, resulting in extraordinary macroscopic properties [1–6].

The thermal behaviour of such copolymers, which is the focus of this work, is, thus, strongly influenced by the comonomer content. In the investigation of Bensason et al. [4] the melting temperature decreases systematically with increasing octene content from 411 K in the homopolymer with a density of 0.955 g cm^{-3} to 331 K in the copolymer with a density of 0.8724 g cm^{-3} (12.3 mol% octene). Additionally, the melting range was broadened towards lower

[1] Current address: Department of Chemistry, The University of Tennessee, Knoxville, TN 37996-1600, USA.

0032-3861/99/$ - see front matter
PII: S0032-3861(98)00470-4

temperatures allowing recrystallization/aging at ambient temperature. For samples with a lower comonomer content, the heat of crystallization showed an increase with decreasing cooling rate, although the heat of fusion was not affected systematically, probably caused by recrystallization/aging at ambient temperature. In copolymers with a higher octene content ($\geq$ 8.2 mol%) no effect of the cooling rate on the thermal behaviour was measured. The recrystallization of ethylene–octene copolymers was investigated in more detail by Minick et al. [7]. Samples were annealed for 1 h at various temperatures within the melting range, quenched to 223 K and characterized via the subsequent differential scanning calorimetry (d.s.c.) heating scan. The occurrence of a broad endotherm below the annealing temperature was assigned to the melting of crystals containing shorter ethylene sequences whereas the relatively sharp as well as a third broad endotherm above the annealing temperature were explained by the incorporation of longer ethylene sequences in crystallites which are present at the annealing temperature. The heat of melting does not vary with the annealing temperature. Earlier d.s.c. studies of the (apparent) heat capacity on different ethylene–octene copolymers (approximately 8 mol% octene) by Mathot et al. [8] have shown that at the glass transition the melting process begins and the crystallization process ends. The appearance of several peaks in the d.s.c. scans in the investigated very low density PE (0.888 g cm^{-3}) was interpreted by the existence of varying amounts of the comonomer in different chains (intermolecular heterogeneity), in contrast to homogeneous copolymers where no multiple peaks were observed. In general, it is assumed that in those copolymers the short chain branches are not incorporated in the crystalline phase, and the two-phase model is widely accepted [4,8]. However, full exclusion of side chains from the (folded chain) crystal is not generally agreed upon [9,10].

Occasionally, d.s.c. traces on PE show a discontinuous crystallization, i.e. a discrete peak and a more or less smooth post-crystallization [8,11,12]. The discontinuous character of the anisothermal process could be explained by secondary crystallization and crystal perfection [13], but less effort has been made to discuss a possible improvement of the order within the remaining amorphous phase or even a crystallization in a separate crystalline phase. These different processes cannot safely be separated due to the phase-integrating character of the d.s.c. method. However, in accordance with the two-step crystallization process observed by d.s.c., additional phases have been found in PE by X-ray scattering [14,15] or Raman spectroscopy [16], and for other polymers, using d.s.c., by the shift of the glass transition temperature due to a changed amount of the so-called rigid–amorphous phase [17]. McFaddin et al. [14] investigated homogeneous ethylene-1-octene copolymers containing 15 mol% 1-octene by wide angle X-ray scattering (WAXS), and could not find any scattering caused by an orthorhombic crystalline phase, but two amorphous bands at 19.7 and 20° (2θ, CuK_α radiation). The peak at 20.0° (2θ) points to a denser structure than the isotropic liquid-like phase (and thus a more ordered phase). Mathot et al. [18] also measured the X-ray diagrams of a homogeneous ethylene–octene copolymer with 13.6 mol% octene content. Probably, due to the slightly lower octene amount the 110 and 200 peaks could be detected very weak as well as a strikingly sharp halo. Regardless the very weak X-ray scattering by the crystalline phase, a crystallinity of 24 and 12% at 233 and 298 K, respectively, was calculated based on d.s.c. data. If the comonomer content is decreased to 9.8 mol% the 110 and 200 reflections were observed, as in standard PE [14].

In this paper heat capacity measurements and temperature-resolved wide angle X-ray measurements on poly (ethylene-*co*-octene) with an octene content of 7.3 mol% are described. The experiments focused on the determination of the temperature range of the melting and the crystallization and its kinetics, and the correlation of macroscopic d.s.c. with structural X-ray data. The heat capacities were measured by conventional d.s.c. and temperature-modulated d.s.c. (TMd.s.c). The TMd.s.c. was primarily used to support the results gathered by d.s.c., but was also applied to get more information about the kinetics of the phase transitions. The temperature-modulation, described by the parameters period, amplitude and underlying heating rate, allows a more accurate determination of the heat capacity and the separation of processes with different kinetics [19–21]. The modulated raw heat-flow data are deconvoluted by Fourier transformation [22] into the total heat flow (caused by the underlying heating rate; the average, corresponding to conventional DSC data) and the reversing heat flow (caused by the modulation; the cyclic component). The difference is the non-reversing heat flow, indicating the contribution of all kinetics events which can not follow the modulation. Empirically it was found that: (1) the glass transition appears in the total and reversing component of the heat flow; (2) the crystallization process appears in the total and non-reversing component, but not in the reversing component of the heat flow; and (3) the melting process may be visible in all three components of the resolved raw data [23]. Whereas the glass transition was investigated quite intensely by TMd.s.c. [21,24–26], this method was applied less often to the melting and crystallization processes. Recently, quasi-isothermal experiments on poly(ethylene terephthalate) [27] and poly(oxyethylene) [28] were published to discuss the melting process by comparing apparent reversing heat capacity data with the expected, theoretical heat capacities. In this work an attempt is made to use TMd.s.c. to elucidate the complicated crystallization and melting behaviour of poly(ethylene-*co*-octene). It is attempted to overcome the main drawback of the d.s.c. method with temperature-resolved WAXS, which is the integrating character of the heat flow signal over the whole sample. In this way, it will be possible to permit the assignment of temperature-induced structural changes in the different phases.

2. Experimental

2.1. Material

A commercial ethylene–octene copolymer (ENGAGE™ 8200) from the DOW Chemical Company was used. The as-received granules were processed at 150°C to films of 0.5 mm thickness. The material was synthesized by the INSITE™ technology and is characterized by the following parameters (Table 1) [1]:

2.2. Instrumentation and experimental details

Conventional d.s.c. and TMd.s.c. were performed on a Mettler Toledo DSC 820. The sample mass was 10 ± 0.5 mg in all experiments. The sample was purged with dry nitrogen at a flow rate of 80 ml min^{-1} (recommended by Mettler Toledo). For cooling, the liquid nitrogen accessory of the device was used. Additionally, the furnace was purged with dry air at a flow rate of 200 ml min^{-1}. Heat capacities by conventional d.s.c. were determined using blind curve subtraction and sapphire calibration. The heating rate was 10 K min^{-1}. TMd.s.c. experiments were performed with a sinusoidal oscillation of the furnace temperature with different modulation parameters as discussed in the text. Preferred parameters are a period of 1.8 min and an amplitude of 1 K. In anisothermal temperature-modulated experiments an underlying heating rate of 1 K min^{-1} was added. Sapphire was used for the heat-flow calibration at least once before or after each run. In general, all experiments were performed several times (depending on the type of experiment). Furthermore, the Mettler Toledo TA 8000 software, with the options (1) heat capacity by sapphire and (2) alternating d.s.c., was applied for data reduction [30].

Wide angle X-ray data (WAXS) were recorded by an URD 63 diffractometer (FPM) using Ni-filtered CuK_α radiation. The measurements were performed in the reflection mode. The diffractometer was equipped with a temperature chamber (Paar KG) and a position-sensitive detector (PSD) (Stoe, FPM). The temperature of the sample holder in the chamber was programmed by a controller. The heating and cooling rate in temperature-dependent experiments was 2 K min^{-1}. All measurements were performed under vacuum. The sample position in heating and cooling experiments was checked using a calibration standard. For data collection and data reduction the software package APX 63 (FPM) was used [31].

Table 1
Characteristics of poly(ethylene-*co*-octene) ENGAGE™ 8200

Comonomer content (wt%)	24
Comonomer content (mol%)	7.3
Density (g cm^{-3})	0.87
Melt flow index (190°C, 2.16 kp) (dg min^{-1})	5
Melt flow ratio (10.0 kp/2.16 kp) (–)	7.1
Dow rheology index[a] (–)	0.5
Molecular weight (g mol^{-1})	78 420[b]
Polydispersity (–)	2.35[b]
Hexyl branches/1000 C (backbone) (–)	36.6
C (backbone)/hexyl branch (–)	27.3

[a]Sensitive to long chain branches [29].
[b]Own data.

3. Results and discussion

Fig. 1 shows the heat capacity of amorphous and crystalline polyethylene in dependence on temperature as documented in the ATHAS data bank [32] and values of poly(ethylene-*co*-octene) measured by conventional d.s.c. during heating and cooling. The measured data represent apparent heat capacities due to possible contributions to the heat flow from enthalpy changes by melting or crystallization [33]. The measurements were performed in a temperature range between 173 and 393 K to get data also at temperatures where definitely no latent heat changes occur. The experimental values below the glass transition (237 K) [34] and in the melt agree well with the data of the ATHAS data bank. Between the glass transition and a temperature where the material is melted, the apparent heat capacity is different from the ATHAS values, indicating possible phase changes. During heating, the melting process seems to start at 240 K, i.e. immediately above the glass transition, and is finished at 355 K (end of melting). The temperature-dependence of the enthalpy-based crystallinity [18,35] was calculated for the second heating scan as shown in Fig. 1. The crystallinity is 24% at 240 K and decreases continuously to a value of 14% at 298 K and finally reaches zero at 355 K (Fig. 2). The crystallization process during cooling (Fig. 1) begins at 323 K (onset) and covers the temperature range down to the glass transition. The crystallization seems to consist of at least two different processes, indicated by the sharp peak at 318 K (maximum) and a more

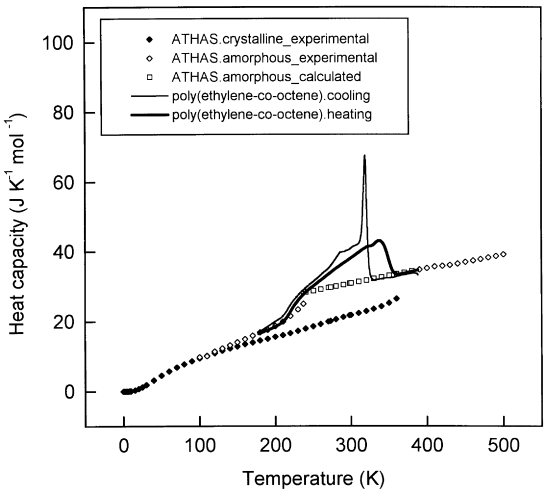

Fig. 1. Heat capacity of poly(ethylene-*co*-octene) in dependence on temperature.

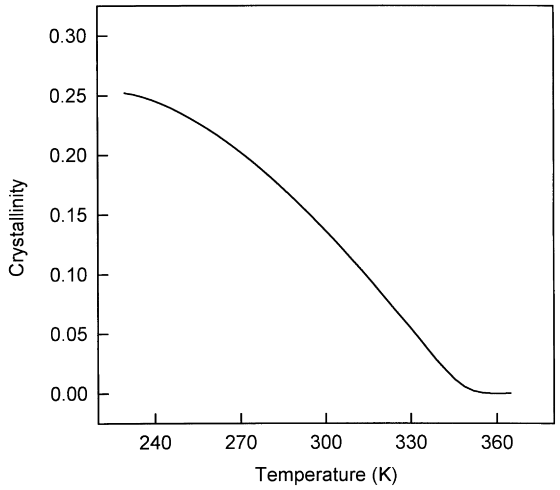

Fig. 2. Temperature dependence of the enthalpy-based crystallinity of poly(ethylene-*co*-octene) during heating.

smoothly running process afterwards. Very weak crystallization peaks can be found at temperatures of about 285 and 290 K which are not reproducible in temperature and heat of crystallization.

Fig. 3 summarizes the influence of thermal history on the melting behaviour of the copolymer. The sample was stored for different times at ambient temperature, resulting in a systematically changed structural state before the subsequent heating scan which starts below the glass transition. Those heating scans show a decrease in the endotherm at approximately 300 K, immediately followed by an increase that develops into a typical annealing peak. With storage time the overall heat of fusion and the temperatures of the annealing peak are shifted to higher values, as shown in Table 2.

The percentage increase of the overall heat fusion ΔH_f for a particular storage time t was calculated by the following

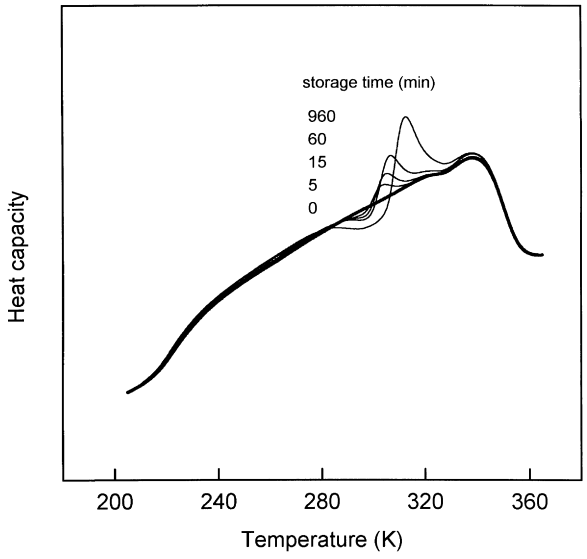

Fig. 3. Standard d.s.c. heating scans of poly(ethylene-*co*-octene) after storing for different times at ambient temperature.

Table 2
Change of the overall heat of fusion (ΔH_f) and of the maximum temperature of the annealing peak (T_a) in dependence on the storage time (t) at ambient temperature

t (min)	ΔH_f (%)	T_a (K)
0	0	–
5	0.4	304.7
15	0.7	305.3
60	1.3	306.8
960	1.7	312.5

equation:

$$\Delta H_f(t) = \frac{\int_{205}^{365} c_p^t(T)dT - \int_{205}^{365} c_p^0(T)dT}{\int_{205}^{365} c_p^0(T)dT} * 100\%$$

In this equation $c_p^t(T)$ is the temperature-dependent heat capacity of the sample which was stored a time t and $c_p^0(T)$ is the temperature-dependent heat capacity of the non-stored sample. The changes with storage time give rise to the assumption that structural rearrangements are possible at room temperature. Obviously, the material is not in equilibrium. One cannot distinguish with certainty between recrystallization and annealing [13] or a mixture of both, but the data in Table 2 suggest that during storing at ambient temperature the crystallinity increases by crystal perfection, i.e. annealing of already existing crystallites. In the case of a recrystallization, the areas of the 'exothermic' and endothermic peak should be equal as well as the overall heat of fusion, which are obviously not. Due to the annealing process before the subsequent heating scan the material is already in a state of higher crystallinity, otherwise the overall heat of fusion would not be larger. The annealing peak occurs at a lower temperature than the main melting at 355 K, probably due to the smaller size of the additional crystallites. An explanation for the downwards shift of the heat flow on heating could be an missing melting endotherm, caused by the changed crystal morphology during annealing. The annealed crystals melt at a higher temperature, as indicated by the additional endotherm at slightly higher temperature (annealing peak). The shift of the annealing peak towards a higher temperature with a longer annealing time also points to crystal perfection and crystal growth rather than the formation of new crystals [36]. The crystals that melt at higher temperatures after longer annealing times are larger and/or more ordered than those formed after shorter annealing times. A simple crystallization into new crystallites of uniform size and order would result in melting at a constant temperature.

The importance of kinetic factors in the crystallization process is substantiated by a distinct dependence of the X-ray crystallinity (at room temperature) on the cooling rate,

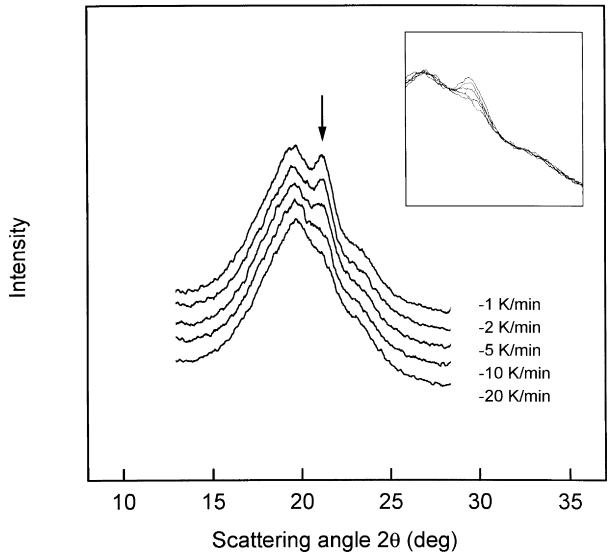

Fig. 4. Wide angle X-ray diagrams of poly(ethylene-*co*-octene) after cooling at the indicated rates.

as is illustrated in Fig. 4. The X-ray diagrams in Fig. 4 were taken immediately after controlled cooling of the samples with the indicated cooling rates. The marked peak, which can be assigned to the (110) lattice plane of the orthorhombic unit cell, decreases in its intensity with increasing cooling rate and disappears almost completely at a cooling rate of 20 K min^{-1}. The result demonstrates the strong influence of the crystal perfection on the kinetics of the crystallization. The d.s.c. scans in dependence on the cooling rate are,

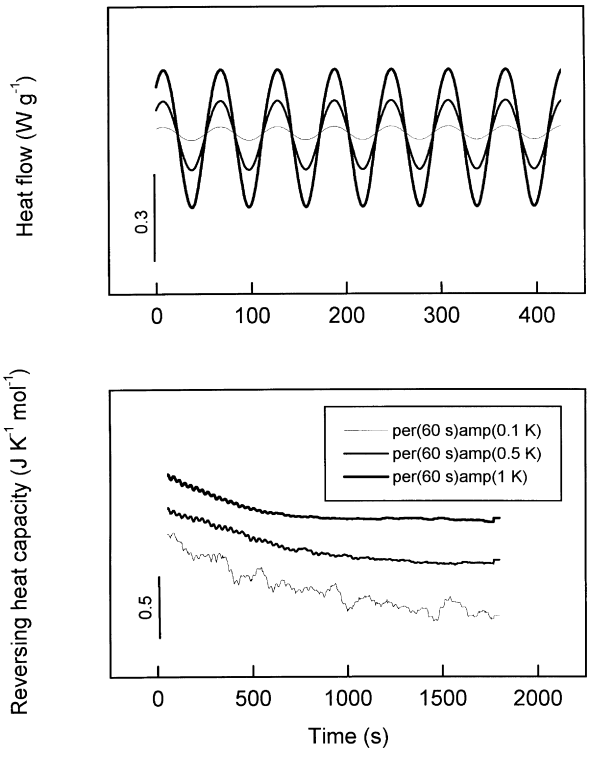

Fig. 5. Modulated heat flow and reversing heat capacity of poly(ethylene-*co*-octene) as a function of modulation amplitude.

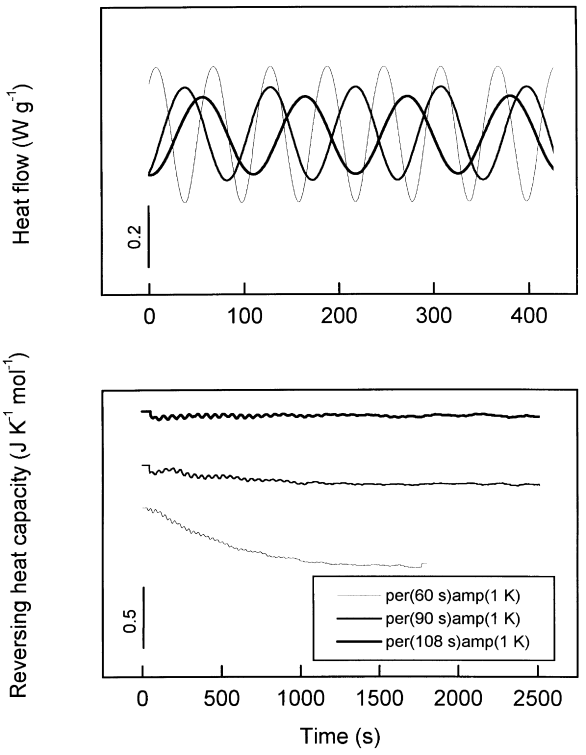

Fig. 6. Modulated heat flow and reversing heat capacity of poly(ethylene-*co*-octene) as a function of modulation period.

in contrast, almost independent on cooling rates, particularly if one considers the main crystallization peak seen in Fig. 1. One must conclude that most of the changes in the X-ray diagram are thus improvements in the crystal structure, rather than a major increase in crystallinity, which would have also been seen by d.s.c.

Figs. 5 and 6 show results of quasi-isothermal TMd.s.c. at 373 K, to identify optimal modulation conditions, i.e. modulation period and amplitude. The choice of correct modulation parameters is a prerequisite to assure steady state, even during the slow structural changes. The tests indicate that with increasing temperature amplitude the noise in the reversing heat capacity is reduced (Fig. 5), and that with an increased period steady state is reached earlier (Fig. 6). Based on these experiments a temperature amplitude of 1 K and a period of 108 s were selected, considering also, that in cooling experiments the rates must be realized down to 173 K. Steady state must also be reached sufficiently fast to separate the different time-dependent processes.

In Fig. 7 plots are shown of the reversing heat capacity measured by TMd.s.c. (thick lines) and standard d.s.c. (thin lines, see also Fig. 1). Heating is indicated by the dashed lines and cooling is represented by solid lines. The total heat capacity from the modulated d.s.c. experiment was not used due to uncertainties in the baseline correction; however, the standard d.s.c. experiment corresponds to the total heat capacity in the modulated scan. It is evident from this plot that during cooling several crystallization processes occur. The discrete peak at the beginning of the crystallization only

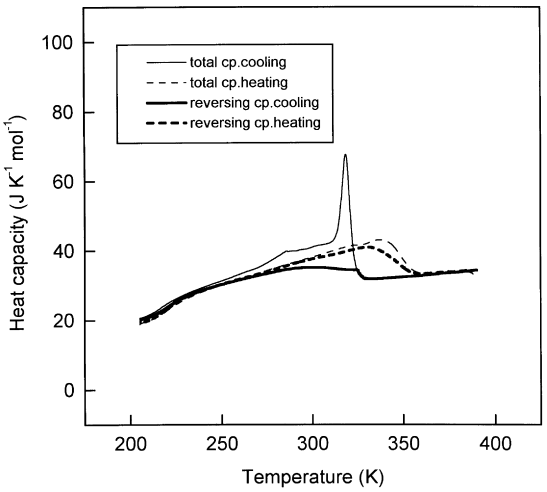

Fig. 7. Heat capacity of poly(ethylene-*co*-octene), measured by TMd.s.c. (reversing heat capacity) and standard d.s.c. (total heat capacity).

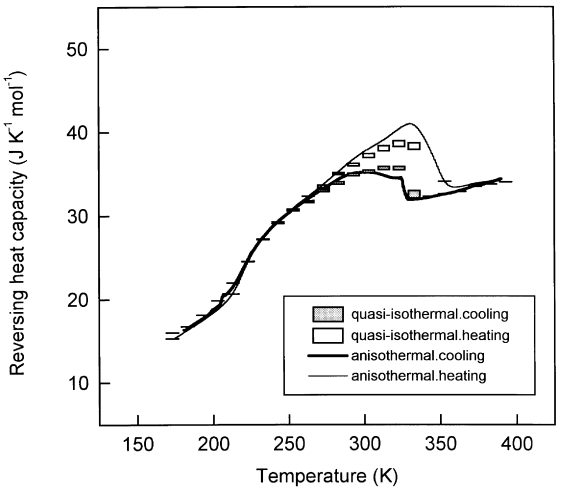

Fig. 8. Reversing heat capacity of poly(ethylene-*co*-octene) measured by standard and quasi-isothermal TMd.s.c.

appears in the total heat capacity and not in the reversing heat capacity, i.e. this process is non-reversible and continues to approximately 255 K (the end of the process cannot unambiguously be defined). However, at approximately 328 K the reversing heat capacity also increases, probably as a result of a second exothermic process which continues over a wide temperature range. This is in contrast to the more frequently measured non-reversing character of the crystallization, especially if the process occurs in a narrow temperature range. However, if the process continues over a wider temperature range even a non-reversing process could contribute to the first harmonic of the Fourier transformation. A periodic heat flow during each cooling cycle would cause additional crystallization by the underlying heating rate. As will be shown below by quasi-isothermal experiments, this contribution can be neglected at temperatures below 300 K. The heating scan supports the assumption of a continuous melting above the glass transition and appears mainly in the reversing component of the heat flow. Larger deviations between the underlying and reversing heat capacity can be seen in the end of the melting process as a separate shoulder. It is straightforward to assume that this melting (with a different kinetics than the continuous melting at lower temperatures) is correlated to the crystallization characterized by a corresponding kinetics, i.e. the first crystallization peak.

In Fig. 8 a comparison is given of quasi-isothermally measured data with standard TMd.s.c. data. In the heating experiment each point was collected using the following temperature program: heating to 393 K, holding 5 min, cooling to 173 K, heating to the final modulation temperature. This temperature program equalizes the thermal history of the sample to make the measurements comparable. Correspondingly, in the cooling experiment the sample was molten before each experiment. In the plot not only a simple point is drawn, rather the change in reversing heat capacity with time. This is necessary since the instrumental and structural steady state is not reached immediately. The bar covers 20 cycles, which corresponds to 36 min (20 cycles $\times$ 108 s period). After this time the heat capacity change is negligible, but not yet constant. In the cooling run at 313 K, the change was $<$1% after 80 additional cycles. The heat capacity decreases with time at each temperature, both in the heating and cooling experiments, except at 333 K in the cooling run (last bar) where there is an increase of the reversing heat capacity, probably indicating continual crystallization. The downwards shift of the heat capacity must be explained by structural changes since the changes due to instrument effects are zero after only few cycles when measurements are made at temperatures outside the transition. In the experiments in the melting/crystallization range the partially reversible character of the crystallization and melting process can be verified. A non-reversible process as considered in the discussion of the reversing heat capacity during cooling in Fig. 7 can now be neglected by avoiding a periodic heat flow due to the

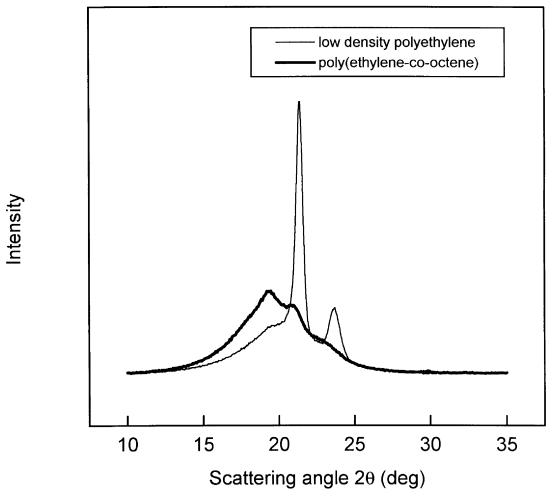

Fig. 9. Wide angle X-ray diagrams of poly(ethylene-*co*-octene) and low-density PE.

underlying heating rate. The percentage to the total change in heat capacity is somewhat larger than in the experiments of Okazaki et al. on PET [27], indicating perhaps a poorer degree of crystallization.

Fig. 9 shows a qualitative comparison of wide angle X-ray scans of poly(ethylene-*co*-octene) to that of conventional, heterogeneous low density PE with a density of 0.92 g cm^{-3}. The peak maximum positions of the 110 and 200 interferences of the orthorhombic unit cell in the case of the low density PE are detected at 21.4° and 23.7° (2θ). These are typical values for low density PE since the unit cell is somewhat enlarged due to incorporated and surface branches [37]. The peaks would appear at 21.66° and 24.05° (2θ) in the case of an undistorted unit cell with the cell parameters $a = 7.400$ Å, $b = 4.930$ Å and $c = 2.534$ Å [38]. In poly(ethylene-*co*-octene) the peaks seem to be shifted to even lower angles, which points to an increased effect of the side-chains on the (orthorhombic) crystalline phase. The amorphous halo is also different from that of low density PE in its shape and position. It can clearly be seen that the amorphous halo of poly(ethylene-*co*-octene) has a sharper or superimposed, additional peak, or a second halo. Assuming the two-phase model of crystalline and amorphous phases would allow to represent the amorphous phase by a single halo in the WAXS diagram. However, several investigations have shown that a strict two-phase model does not mirror the real structure within a semi-crystalline polymer and that different mesophases, including the rigid amorphous phase [39] and the disordered pseudo-hexagonal phase [40] with a lateral long range order, can exist. Also, it was found that the position of the amorphous halo at ambient temperature, usually set to 19.3° (2θ) [41], is higher than the linearly extrapolated value from measurements in the molten state. In the case of low density PE, the crystallization-induced changes of the structure of the amorphous phase can be verified: the position of the amorphous halo was determined by profile fitting to be at 19.9° (2θ); in the case of poly(ethylene-*co*-octene) the profile fitting procedure was not performed to avoid over-interpretation of the data and additional sources of errors due to the increased number of fitting parameters, as well as missing starting values for the nonlinear fitting procedure. On basis of the presented X-ray data, final conclusions about the nature and cause of the amorphous halo or peak, respectively, cannot be drawn. WAXS experiments on oriented samples are in progress and give further information [42].

Temperature-resolved WAXS experiments (Fig. 10) support the existence of an amorphous–crystalline interphase, indicated by the additional peak or halo, respectively. In the heating and cooling experiment, the sample temperature was changed continuously with a rate of 2 K min^{-1}, i.e. each scan covers 4 K. The thick lines are the diagrams at 371, 293 and 246 K in the cooling experiment and 205, 293 and 371 K in the heating experiment. The first diagram in the cooling experiment at 371 K shows only an amorphous halo. The material is in the molten state. At about 321 K the

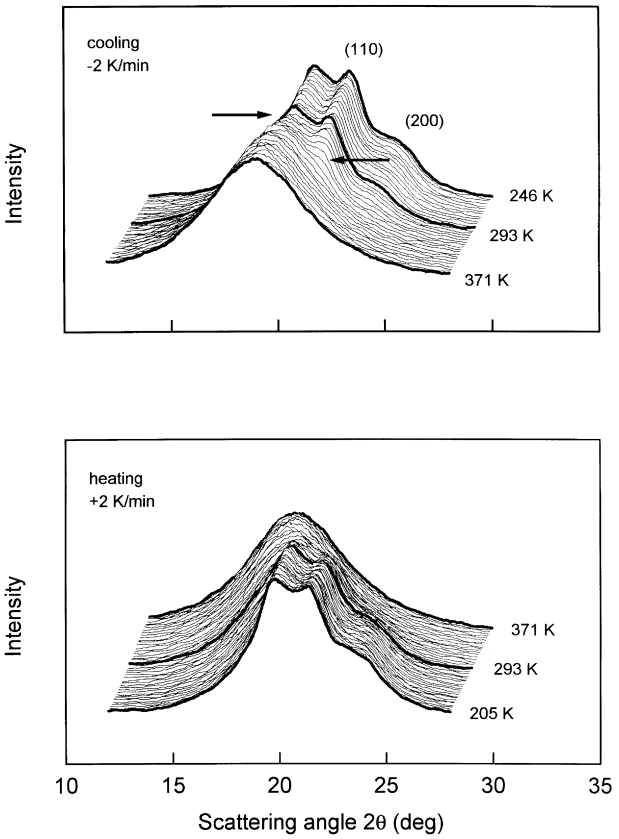

Fig. 10. Wide angle X-ray diagrams of poly(ethylene-*co*-octene) in dependence on temperature during cooling and heating.

110 and 200 interferences appear. At slightly lower temperatures, the shape of the amorphous halo changes abruptly and gets superimposed by the additional peak (see the arrows in Fig. 10). Cooling the sample below ambient temperature results in an increase of the integral intensities of the 110 and 200 interferences as well as of the peak due to the amorphous–crystalline interphase. The increase of the intensities of the 110 and 200 interferences caused by the crystalline phase as well as the strong decrease of the half-width of the amorphous halo is evident also in other polyethylenes, and is not necessarily a typical characteristic of the copolymer [12]. However, an explicit maximum, as measured in the case of poly(ethylene-*co*-octene), was not observed as clearly in the case of conventional PE. It is likely that the occurrence of this maximum is an effect of the exceptionally low X-ray crystallinity.

The intensities of all peaks increase during cooling. This is not caused by further crystallization (in the sense of the transition: amorphous to crystalline phase), rather by an improvement of the internal order. This is unambiguously proved by the heating experiment, which is characterized by a continuous decrease of the intensity of the peaks, i.e. the state of order in the crystalline phase as well as in the mesophase is in equilibrium with temperature. This process is similar to the effects observed by d.s.c. where the (quasi-isothermal reversing) heat capacity is higher than the

expected theoretical value, indicating reversible structural changes in the sample.

4. Conclusions

The experiments presented in this paper have shown the complex character of the melting and crystallization process in commercially available poly(ethylene-*co*-octene). The crystallization is at least a two-fold process, starting with the formation of a crystalline phase followed by the perfection of the grown crystallites and the development of a mesophase. The latter process depends on temperature and continues down to the glass transition. The formation of the crystalline phase and the development of a second, probably less ordered, phase do have different kinetics and thermodynamics, as revealed by TMd.s.c. The melting process starts at the glass transition as a reversing transition, and is finished at 355 K after irreversible melting of the originally grown crystallites.

Acknowledgements

The author thanks Prof. B. Wunderlich for helpful discussions and M. Pyda for the calculation of the enthalpy-based crystallinity.

References

[1] Engage Polyolefine Elastomers, Product Information, Dow Plastics.
[2] Sylvest RT, Lancester G, Betso SR. Kautschuk Gummi Kunststoffe 1997;50 (3):186.
[3] Batistini A. Macromol Symp 1995;100:137.
[4] Bensason S, Minick J, Moet A, Chum S, Hiltner A, Baer E. J Polym Sci, Polym Phys 1996;34:1301.
[5] Sehanobish K, Patel RM, Croft BA, Chum SP, Kao CI. J Appl Polym Sci 1994;51:887.
[6] Bensason S, Stepanov EV, Chum S, Hiltner A, Baer E. Macromolecules 1997;30:2436.
[7] Minick J, Moet A, Hiltner A, Baer E, Chum SP. J Appl Polym Sci 1995;58:1371.
[8] Mathot VBF, Pijpers MFJ. J Appl Polym Sci 1990;39:979.
[9] Seguela R, Rietsch F. J Polym Sci, Polym Letters 1986;24:29.
[10] Vonk CG, Pijpers AP. J Polym Sci, Polym Phys 1985;23:2517.
[11] TA Instruments Publication No. TA 227.
[12] Androsch R, unpublished data.
[13] Wunderlich B. Macromolecular physics, vol. 2, crystal nucleation, growth, annealing. New York: Academic Press, 1976.
[14] McFaddin DC, Russell KE, Wu G, Heyding RD. J Polym Sci, Polym Phys 1993;31:175.
[15] Strobl GR, Hagedorn W. J Polym Sci, Polym Phys 1978;16:1181.
[16] Glotin M, Mandelkern L. Colloid and Polym Sci 1982;260:1982.
[17] Cheng SZD, Pan R, Wunderlich B. Makrom Chemie 1988;189: 2443.
[18] Mathot VBF, Scherrenberg RL, Pijpers MFJ, Bras W. J Thermal Anal 1996;46:681.
[19] Wunderlich B, Jin Y, Boller A. Thermochim Acta 1994;238:277.
[20] Boller A, Jin Y, Wunderlich B. J Thermal Anal 1994;42:307.
[21] Boller A, Schick C, Wunderlich B. Thermochim Acta 1995;266:97.
[22] Wunderlich B. J Thermal Anal 1997;48:207.
[23] Reading M. Thermochim Acta 1994;238:295.
[24] Wunderlich B, Boller A, Okazaki I, Kreitmeier S. J Thermal Anal 1996;47:1013.
[25] Boller A, Okazaki I, Wunderlich B. Thermochim Acta 1996;284:1.
[26] Okazaki I, Wunderlich B. J Thermal Anal 1997;49:57.
[27] Okazaki I, Wunderlich B. Macromolecules 1997;30:1758.
[28] Wunderlich B, Okazaki I, Ishikiriyama K, Boller A. Thermochim Acta, to be published.
[29] Lai S, Plumley TA, Butler TI, Knight GW, Kao CI. Proceedings, SPE ANTEC 1994, 1814.
[30] Manual, Mettler Toledo TA 8000 Software V3.0, Chapters 11.2 and 11.4.
[31] Software package APX63/Powder V2.00/3.00 (Data Collection/Data Reduction), Freiberg, 1992.
[32] AdvancedTHermalAnalysiS data bank, WWW (Internet), http://funnelweb.utcc.utk.edu/~athas/databank/alkene/pe/peexpcr.html and /peexpam.html.
[33] Wunderlich B. Macromolecular physics, vol. 1, crystal structure, morphology, defects. New York: Academic Press, 1973.
[34] Gaur U, Wunderlich B. Macromolecules 1980;13:445.
[35] Pyda M, Wunderlich B. J Thermal Anal, submitted.
[36] Wunderlich B. Macromolecular physics, vol. 3, crystal melting. New York: Academic Press, 1981.
[37] Balta-Calleja FJ, Vonk CG. X-ray scattering of synthetic polymers. Amsterdam: Elsevier, 1989.
[38] Alexander LE. X-ray diffraction methods in polymer science. New York: Wiley-Interscience, 1969.
[39] Menczel J, Wunderlich B. J Polym Sci, Polym Letters 1981;19:261.
[40] Ballasteros OR, Auriemma F, Guerra G, Corradini P. Macromolecules 1996;29:7141.
[41] Hermans PH, Weidinger A. Makromol Chem (Vol. 44–46) 1961:24.
[42] Androsch R, Blackwell J, Chvalun SN, Wunderlich B, submitted.